Narrowband Interference Suppression in Time-Hopping Impulse Radio Ultra-Wideband Communications

Jiangzhou Wang, *Senior Member, IEEE*, and Wong Tat Tung

***Abstract*—Ultra-wideband (UWB) technology has been considered an innovative solution for future short-range high-speed wireless communications. Interference suppression is important for the UWB devices to operate over spectrum occupied by narrowband systems. In this paper, the use of a notch filter in time-hopping impulse radio (TH-IR) for UWB communication is considered, where a Gaussian monopulse is employed with pulse position modulation. Lognormal channel fading is assumed, and a complete analytical framework is provided for the performance evaluation of using a transversal-type notch filter to reject narrowband interference (NBI). A closed-form expression of bit-error probability is derived, and the numerical results show that the use of a notch filter can improve the system performance significantly. Furthermore, a performance comparison between TH-IR and multicarrier code-division multiple-access (MC-CDMA) UWB systems is made under the conditions of the same transmit power, the same data rate, and the same bandwidth. It is shown that in the presence of NBI, the TH-IR system and MC-CDMA system achieve similar performance when both use a notch filter.**

***Index Terms*—Impulse radio (IR), log-normal fading, multicarrier code-division multiple access (MC-CDMA), notch filter, Rake receiver, time-hopping (TH), ultra-wideband (UWB) communications.**

I. Introduction

OVER THE LAST decade, there has been a great interest in ultra-wideband (UWB) time-hopping (TH) impulse radio (IR) communication systems [1]–[8]. These systems make use of ultra-short duration pulses (monocycles) which yield ultra-wide bandwidth signals characterized by extremely low power densities. UWB systems are particularly promising for short-range high-speed wireless communications, as they potentially combine reduced complexity with low power consumption, low probability of intercept, high-accuracy positioning, and immunity to multipath fading due to discontinuous transmission. Recently, the Federal Communications Commission (FCC) has defined the −10 dB emission mask between 3.1–10.6 GHz for the unlicensed UWB systems with bandwidth of at least 500 MHz [9]. However, in this frequency band, there are a variety of existing narrowband interfering signals, such as a public safety band and wireless LAN (IEEE 802.11a) operating at frequencies of 4.9 and 5.2 GHz, respectively. This means that UWB signals and narrowband signals must coexist, and minimal mutual interference between them must be ensured. Therefore, the successful deployment of the UWB technology depends not only on the development of efficient multiple-access techniques, but also on narrowband interference (NBI) suppression techniques. Since the receiver of TH-IR is operated by time gating matched to the pulse duration [1]–[3], this time gating reduces the power of continuous-time interference to the duty cycle of IR. Therefore, TH-IR inherently has the capability of NBI suppression. However, when NBI is very strong, we may need to use a notch filter [17] to help to reject it.

Suppression schemes based on minimum mean-square error (MMSE) Rake combining were proposed in [10] and [11], while the computation complexity of the tap weight would be increased with addition of branches within the Rake receiver as it is driven by the decision statistic. In this paper, we study the use of a notch filter to suppress NBI for TH-IR. A notch filter has been widely studied to reject NBI for code-division multiple-access (CDMA) overlay systems when NBI is very strong [15]. Apart from the higher sampling-speed requirement in comparison with the solutions proposed in [10] and [11], since the computation of the tap weights for notch filter depends on the nature of the narrowband interferer, the same set of weights determined from well training can be adopted among the branches with the Rake receiver. Moreover, notch filter also offers flexibility, as its narrowband rejection ability can be enhanced by the addition of more taps. In our work, we provide a complete performance analysis of error probability in addition to the simulation result.

The UWB concept can be based on several techniques, such as TH-IR or multicarrier CDMA (MC-CDMA) techniques. In the proposed MC-CDMA system for UWB [14], a notch filter has been shown to be very effective in rejecting narrowband signals. For the two different systems (TH-IR and MC-CDMA), we will compare their performances with a notch filter, assuming that they have the same transmit power, the same data rate, and the same bandwidth. The paper is organized as follows. The system models, including transmitter, NBI, channel response, and receiver are described in Section II. In Section III, the bit-error rate (BER) performance is analyzed and a closed-form expression for the BER is given. Section IV presents representative numerical results of system performance under various conditions. Section V gives the performance comparison of TH-IR and MC-CDMA, and finally, Section VI draws the conclusions.

II. System Models

Suppose the time scale is divided into frames with duration T_f, and each frame is composed of N_h slots of duration T_c. The transmitted signal of the kth UWB user employing TH-IR with

Paper approved by A. Zanella, the Editor for Wireless Systems of the IEEE Communications Society. Manuscript received July 13, 2004; revised September 21, 2005.

J. Wang is with the Department of Electronics, University of Kent, Kent CT2 7NT, U.K. (e-mail: j.z.wang@kent.ac.uk).

W. T. Tung is with the Department of Electrical and Electronic Engineering, University of Hong Kong, Hong Kong (e-mail: ttwong@eee.hku.hk).

Digital Object Identifier 10.1109/TCOMM.2006.876855

pulse position modulation (PPM) is given by

$$s_k(t) = \sum_{n=-\infty}^{\infty} \sqrt{E_k}\Xi\left(t - nT_f - c_k^{(n)}T_c - \varepsilon d_k^{\lfloor n/N_s \rfloor}\right) \quad (1)$$

where E_k is the energy of a pulse and $\Xi(t)$ is the shape of the transmitted pulse. $\{c_k^{(n)}\}$ is the TH code of the kth user, where $c_k^{(n)} \in \{0, 1, \ldots, N_h - 1\}$, such that an additional time shift of $c_k^{(n)}T_c$ is introduced when the nth pulse of the kth user is transmitted. The code sequences of all users are assumed to be mutually independent. N_s is the number of pulses transmitted per symbol, i.e., the processing gain, the modulating data symbol changes every N_s hops (frames), and the index of the data symbol is $\lfloor n/N_s \rfloor$ ($\lfloor x \rfloor$ is the integer part of x). $\{d_k^{\lfloor n/N_s \rfloor}\}$ is the binary data sequence of the kth user and composed of equally likely symbols (or bits). A symbol has duration $T_s = N_sT_f$, and the symbol rate is $R_s = 1/T_s = 1/(N_sT_f)$. ε is the modulation index where it is assumed that $\varepsilon > 0$ and $T_p + \varepsilon \leq T_c$, where T_p denotes the pulse width, and the time shift added to a pulse by data is $\varepsilon d_k^{\lfloor n/N_s \rfloor}$. The optimal value of ε is around 20% of a pulse width [7].

In this paper, the monocycle denoted by $\Xi(t)$ is assumed to be a scaled second derivative of the Gaussian function with unit energy, i.e., $\int_{-\infty}^{+\infty} \Xi^2(t)dt = 1$, and one form of a Gaussian monocycle in [8] is adopted as

$$\Xi(t + T_p/2) = \sqrt{\frac{28}{3T_p\sqrt{\pi}}}\left[1 - \left(\frac{7t}{T_p}\right)^2\right]\exp\left[-\frac{1}{2}\left(\frac{7t}{T_p}\right)^2\right] \quad (2)$$

and the -10 dB bandwidth of the Gaussian pulse is approximately given by

$$B_{\text{uwb}} \approx 3.185/T_p. \quad (3)$$

Fig. 1 shows a sample of UWB transmitted signal, where $N_s = 3$ and $N_h = 4$.

The narrowband interferer $j(t)$ is assumed to be passband Gaussian with center frequency f_j and bandwidth B_j. The double-sided flat power spectral density (PSD) of the narrowband interferer is given by

$$S_j(f) = \begin{cases} J/(2B_j), & |f \pm f_j| \leq B_j/2 \\ 0, & \text{otherwise} \end{cases} \quad (4)$$

where J is the power of the NBI, and the autocorrelation function of $j(t)$ is

$$\begin{aligned} R_j(\tau) &= \int_{-\infty}^{\infty} S_j(f)\exp(j2\pi f\tau)df \\ &= J \cdot \overline{R}_j(\tau) \end{aligned} \quad (5)$$

where $\overline{R}_j(\tau)$ denotes the normalized autocorrelation function of $j(t)$, given by

$$\overline{R}_j(\tau) = \frac{\sin(\pi B_j\tau)}{\pi B_j\tau}\cos(2\pi f_j\tau). \quad (6)$$

For the uniformity in comparison with MC-CDMA in later sessions, the parameter p is defined as a ratio of the bandwidth

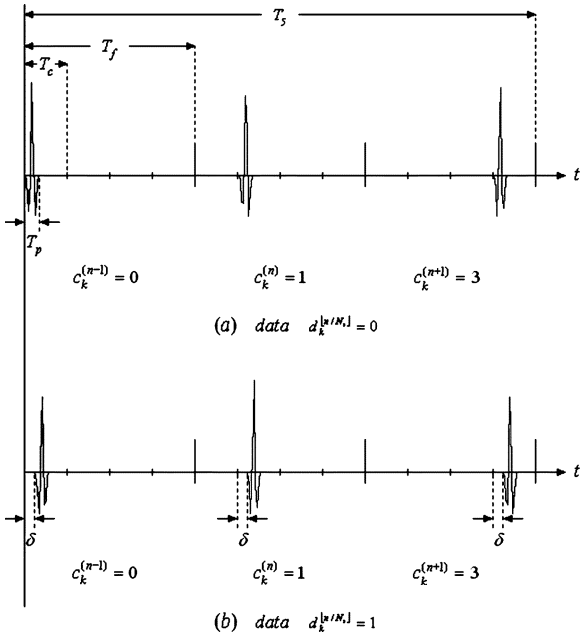

Fig. 1. Sample of UWB TH-IR waveform ($N_s = 3$ frames, $N_h = 4$ bins).

of the narrowband signal to the -10 dB bandwidth, B_{uwb}, of the Gaussian pulse, which can be written as

$$p = B_j/B_{\text{uwb}}. \quad (7)$$

For a typical narrowband system, the usual range of the ratio should be $0 \leq p \ll 0.1$. Another important parameter, q, is defined as a ratio of the difference in center frequencies (between the narrowband interferer and the Gaussian pulse) to the bandwidth of the Gaussian pulse, given by

$$q = (f_j - f_{\text{uwb}})/B_{\text{uwb}} \quad (8)$$

where $-0.5 \leq q \leq 0.5$. In (8), f_{uwb} is the center frequency of the spectrum of the Gaussian pulse, and $f_{\text{uwb}} \approx B_{\text{uwb}}/2$. Therefore, the parameter q can be written approximately as

$$\begin{aligned} q &= \left(f_j - \frac{B_{\text{uwb}}}{2}\right)\Big/B_{\text{uwb}} \\ &= f_j/B_{\text{uwb}} - \frac{1}{2}. \end{aligned} \quad (9)$$

The realistic UWB channel should be a dense multipath fading channel [7]. More than a dozen resolvable paths should exist. In the multiple-access system with K users, the received signal can be expressed as

$$r(t) = \sum_{k=1}^{K}\sum_{l=1}^{L}\psi_{k,l}\beta_{k,l}s_k(t - \tau_{k,l}) + j(t) + n(t) \quad (10)$$

where $\psi_{k,l}$, $\beta_{k,l}$, and $\tau_{k,l}$ represent the phase, amplitude attenuation, and delay, respectively, of the lth arrival path of the kth user. Independent fading is assumed for each path, as well as for each user [16]. The phases are independent variables and take the value 1 or -1 with equal probability to account for signal inversion due to reflection. The delay is assumed to be uniformly

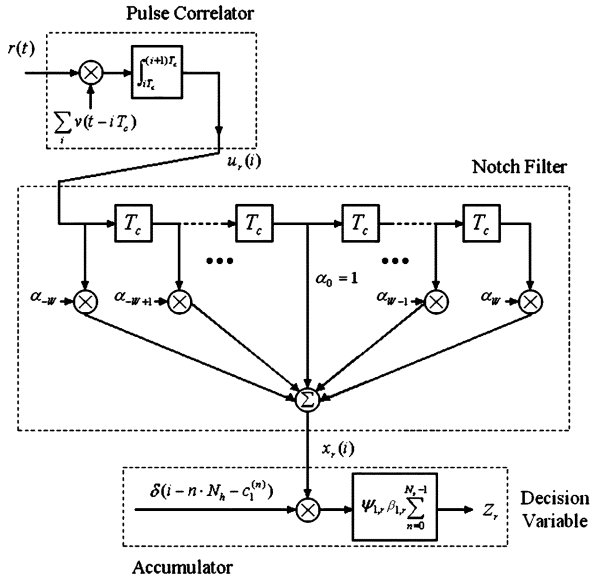

Fig. 2. The rth branch of the receiver.

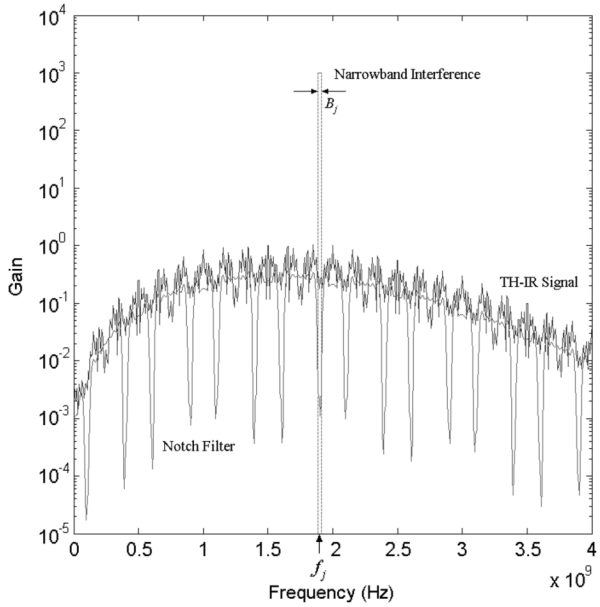

Fig. 3. Frequency responses of the transmitted TH-IR signal and the notch filter at receiver.

distributed over $[0, T_s)$, i.e., the symbol duration. The amplitude attenuation is log-normally distributed with $\mu_{k,l}$ and $\sigma_{k,l}$ being the mean and standard derivation, respectively, its probability density function (pdf) takes the form

$$p(\beta_{k,l}) = \frac{1}{\beta_{k,l}\sigma_{k,l}\sqrt{2\pi}} \exp\left\{\frac{-[\ln(\beta_{k,l}) - \mu_{k,l}]^2}{2\sigma_{k,l}^2}\right\} \quad (11)$$

and its normalized intensity profile is given by

$$\Omega_{k,l} = E\left[\beta_{k,l}^2\right] = \frac{1-\exp(-\nu)}{1-\exp(-L\nu)} \exp\left[-(l-1)\nu\right] \quad (12)$$

where ν is the decay rate. Note that the normalization implies that the sum of the attenuation power of all paths is one ($\sum_{l=1}^{L} \Omega_{k,l} = 1$). In (10), $n(t)$ is an additive white Gaussian noise (AWGN) with double-sided PSD of $\eta_o/2$.

III. Performance Evaluation

Selective maximal combination (SMC) is considered for the proposed receiver design, where R highest ($R < L$) power paths out of all resolvable paths chosen for decision making. Perfect power control is also assumed. As shown in Fig. 2, each branch of the Rake receiver consists of a pulse correlator, a notch filter, and an accumulator. Assuming that the first user is the desired user, the output of the pulse correlator for the rth selected path is given by

$$\begin{aligned} u_r(i) &= \int_{iT_c}^{(i+1)T_c} r(t) \sum_i v(t - iT_c - \tau_{1,r}) dt \\ &= \int_0^{T_c} r(t + iT_c + \tau_{1,r}) v(t) dt \end{aligned} \quad (13)$$

where $v(t)$ is the template pulse function, defined as

$$v(t) = \Xi(t) - \Xi(t - \varepsilon). \quad (14)$$

Note that the pulse correlator output is sampled at the rate of one sample per bin period T_c. The notch filter (Wiener filter) is used to predict and notch out the NBI [17]. The number of taps on each side of the notch filter is W, and thus, the total number of taps is $2W + 1$. The coefficients of the filter are $\{\alpha_w\}$ with $w = [-W, \cdots, W]$ and $\alpha_0 = 1$. Note that when there is no NBI, the filter reduces to an all-pass filter, i.e., $\alpha_w = 0$ for $w \neq 0$. The conceptual frequency response of the notch filter along with the spectra of TH-IR signal and NBI are shown in Fig. 3, which shows that the NBI can be suppressed. The output of the notch filter can be expressed as

$$\begin{aligned} x_r(i) &= \sum_{w=-W}^{W} \alpha_w u_r(i - w) \\ &= \sum_{w=-W}^{W} \alpha_w \int_0^{T_c} r(t - wT_c + iT_c + \tau_{1,r}) v(t) dt. \end{aligned} \quad (15)$$

This output is passed to the accumulator using a delta function $\delta(i - nN_h - c_1^{(n)})$, where $\delta(i) = 1, 0$ for $i = 0$ and $i \neq 0$, respectively. Thus, with the multiplication, the phase $\psi_{1,r}$, and the amplitude attenuation $\beta_{1,r}$ perfectly estimated from the channel, the random variable at the output of the accumulator is given by

$$\begin{aligned} Z_r &= \beta_{1,r}\psi_{1,r} \sum_{i=-\infty}^{\infty} \sum_{n=0}^{N_s-1} x_r(i) \cdot \delta\left(i - nN_h - c_1^{(n)}\right) \\ &= \beta_{1,r}\psi_{1,r} \sum_{n=0}^{N_s-1} x_r\left(nN_h + c_1^{(n)}\right) \\ &= \beta_{1,r}\psi_{1,r} \\ &\quad \times \sum_{n=0}^{N_s-1} \left[\sum_{w=-W}^{W} \alpha_w \int_0^{T_c} r\Big(t - wT_c + nT_f \right. \\ &\quad \left. + c_1^{(n)}T_c + \tau_{1,r}\Big) v(t) dt \right] \\ &= Z_{D|r} + Z_{I|r}. \end{aligned} \quad (16)$$

$Z_{D|r}$ is the desired signal term from the rth selected path for the first user and from the central tap of the notch filter, and is given by

$$\begin{aligned} Z_{D|r} &= \sum_{n=0}^{N_s-1} \beta_{1,r}^2 \psi_{1,r}^2 \int_0^{T_c} s_1\left(t + nT_f + c_1^{(n)} T_c\right) v(t)dt \\ &= \sqrt{E_1}\beta_{1,r}^2 \sum_{n=0}^{N_s-1} \int_0^{T_c} \Xi\left(t - \varepsilon d_1^{\lfloor n/N_s \rfloor}\right) v(t)dt \\ &= \begin{cases} \sqrt{E_1}\beta_{1,r}^2 N_s \rho, & \text{for } d_1^{\lfloor n/N_s \rfloor} = 0 \\ -\sqrt{E_1}\beta_{1,r}^2 N_s \rho, & \text{for } d_1^{\lfloor n/N_s \rfloor} = 1 \end{cases} \end{aligned} \tag{17}$$

where ρ stands for the correlation between the transmitted pulse and the template function

$$\begin{aligned} \rho &= \int_0^{T_c} \Xi(t) v(t)dt \\ &\approx -\int_0^{T_c} \Xi(t) v(t-\varepsilon)dt. \end{aligned} \tag{18}$$

$Z_{I|r}$ in (16) is the total interference for the rth selected path given by

$$Z_{I|r} = Z_{\mathrm{MPI}|r} + Z_{\mathrm{MAI}|r} + Z_{\mathrm{NBI}|r} + Z_{\mathrm{AWGN}|r} \tag{19}$$

where $Z_{\mathrm{MPI}|r}$ is the multipath interference (MPI) from other paths of the desired user, $Z_{\mathrm{MAI}|r}$ is the multiple-access interference (MAI) from all other $K-1$ interfering users, $Z_{\mathrm{NBI}|r}$ is the NBI, and $Z_{\mathrm{AWGN}|r}$ is the AWGN. Note that the disturbance (self-interference) caused by the notch filter to the desired user (or interference of the desired user caused by the non-central taps of the notch filter) should be very small when the bandwidth ratio p is small [15]. Including this interference makes the analysis very complicated since this term contains the same fading factors as the desired term, so self-interference is neglected in (19) for simple analysis. Since the terms in (19) are independent when the number of multipaths is large, the total interference can be approximated as Gaussian with variance

$$\begin{aligned} \mathrm{Var}[Z_{I|r}] = \mathrm{Var}[Z_{\mathrm{MPI}|r}] + \mathrm{Var}[Z_{\mathrm{MAI}|r}] + \mathrm{Var}[Z_{\mathrm{NBI}|r}] \\ + \mathrm{Var}[Z_{\mathrm{AWGN}|r}] \end{aligned} \tag{20}$$

where $\mathrm{Var}[Z_{\mathrm{MPI}|r}]$, $\mathrm{Var}[Z_{\mathrm{MAI}|r}]$, and $\mathrm{Var}[Z_{\mathrm{NBI}|r}]$ stand for the variances of the MPI, MAI, and the NBI, respectively, derived in Appendices A, B, and C, respectively, and are given by (A11), (B10), and (C6), respectively. $\mathrm{Var}[Z_{\mathrm{AWGN}|r}]$ stands for the variance of the noise term, given by

$$\mathrm{Var}(Z_{\mathrm{AWGN}|r}) = \eta_o \beta_{1,r}^2 \sigma_{\mathrm{AWGN}|r}^2 \tag{21}$$

where

$$\sigma_{\mathrm{AWGN}|r}^2 = \frac{N_s}{2}\left(\sum_{w=-W}^{W} \alpha_w^2\right)\left(\int_0^{T_c} v^2(t)dt\right). \tag{22}$$

Therefore, after weighting by amplitude attenuation, the signal-to-interference-plus-noise ratio (SINR) in Z_r is given by

$$\begin{aligned} \gamma_r &= \frac{E^2[Z_r]}{\mathrm{Var}[Z_r]} \\ &= \beta_{1,r}^2 \left\{ \frac{\sigma_{\mathrm{MPI}|r}^2}{N_s^2\rho^2} + \frac{(K-1)\sigma_{\mathrm{MAI}|r}^2}{N_s^2\rho^2} + \left(\frac{J}{P}\right)\frac{\sigma_{\mathrm{NBI}|r}^2}{N_s^2\rho^2 N_h T_c} \right. \\ &\qquad \left. + \left(\frac{E_b}{\eta_o}\right)^{-1} \frac{\sigma_{\mathrm{AWGN}|r}^2}{N_s\rho^2} \right\}^{-1} \\ &= \beta_{1,r}^2 \bar{\gamma}_r \end{aligned} \tag{23}$$

where $\bar{\gamma}_r$ is the average SINR excluding the amplitude attenuation $\beta_{1,r}$, $E_b = E_1 N_s$ denotes the received bit energy, and $P = E_1/(N_h T_c)$ represents the average transmitted power of the UWB signal. The outputs from the R selected branches of the Rake receiver are combined, so the decision variable is given by

$$Z = \sum_{r=1}^{R} Z_r \tag{24}$$

with SINR

$$\gamma = \sum_{r=1}^{R} \beta_{1,r}^2 \bar{\gamma}_r. \tag{25}$$

Since the square of a log-normal random variable is still log-normal distributed, by Schwartz and Yeh's method [18], the distribution of the sum of log-normal random variables can be approximated by another log-normal distribution. Its mean and variance can be obtained by a recursive approach from the individual mean and standard derivation of the attenuation factors. Defining $\bar{\gamma}_{\mathrm{ave}} = (1/R)\sum_{r=1}^{R} \bar{\gamma}_r$ as the mean of the average SINR excluding the attenuation factor for all selected paths, and $\zeta = \sum_{r=1}^{R} \beta_r^2$ as the sum of the square of the attenuation factors, the error probability can be approximated as

$$\begin{aligned} P_e &= \int_0^{\infty} Q(\sqrt{\gamma}) p(\gamma) d\gamma \\ &\approx \int_0^{\infty} Q(\sqrt{\zeta \bar{\gamma}_{\mathrm{ave}}}) p(\zeta) d\zeta \end{aligned} \tag{26}$$

where the Q-function $Q(x)$ is defined as

$$Q(x) = \frac{1}{\sqrt{2\pi}} \int_x^{\infty} \exp(-\Theta^2/2) d\Theta. \tag{27}$$

IV. Comparison of TH and MC-CDMA

In order to compare the TH system with the MC-CDMA in the presence of NBI, we briefly describe the MC-CDMA, which was studied in [14]. MC-CDMA modulates different subcarriers using the same data. All subcarrier spectra are disjoint. The MC-CDMA has an inherent frequency diversity capability

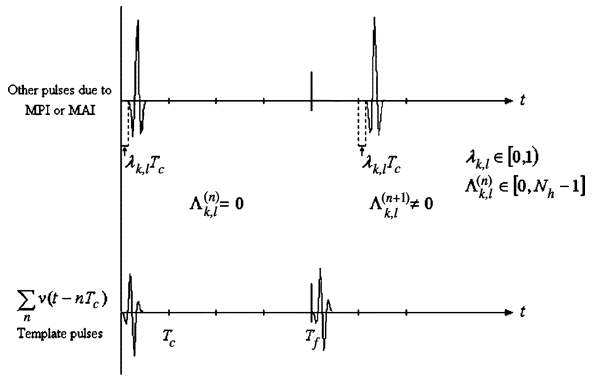

Fig. 4. Illustration of pulse interference.

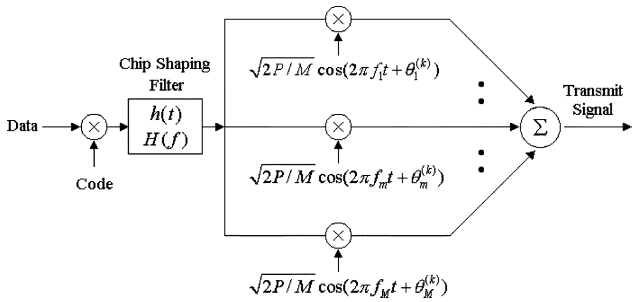

Fig. 5. Transmitter for the kth user of the MC-CDMA UWB system.

by combining the outputs of the different subcarrier signals at the receiver. Moreover, it yields effective NBI rejection in an overlay mode. For example, when there is a strong narrowband interferer in one of the subbands, in the worst case, the receiver can simply ignore the signal in that subcarrier band. An effective way is to use a notch filter to suppress NBI in each subcarrier. Then, even a jammed subcarrier signal can still make a positive contribution to the net frequency diversity.

The pulse interference is shown in Fig. 4. Fig. 5 illustrates the transmitter of the MC-CDMA system. The source binary data sequence is first spread by the random binary sequence. Then, the spread signal is shaped by a chip-waveform shaping filter (square-root raised cosine filter of rolloff factor ϑ) with frequency response $H(f)$. After that, the shaped signal modulates M different subcarriers. Finally, the M subcarrier modulated signals are summed to form a transmitter signal.

For fair comparison, the channel parameters have to be chosen appropriately, as each subband of MC-CDMA occupies only a portion of the bandwidth of the UWB system. It is assumed that the number of paths in each subcarrier is $L_{\mathrm{MC}} = L/M$. That is, each subband of the MC-CDMA would have fewer multipaths, but of greater power with a larger decay rate than the TH-IR system. In addition, the phase of each path is no longer a binary, but a random, variable uniformly distributed over $[0, 2\pi)$, due to the introduction of the carrier.

As shown in Fig. 6, the receiver consists of M parallel branches of the Rake receiver with R correlators, corresponding to M subcarriers. In each branch, the received signal is input to a frequency down converter. After that, a baseband matched filter with frequency response $H^*(f)$ is employed. Then, the output of the matched filter passes through

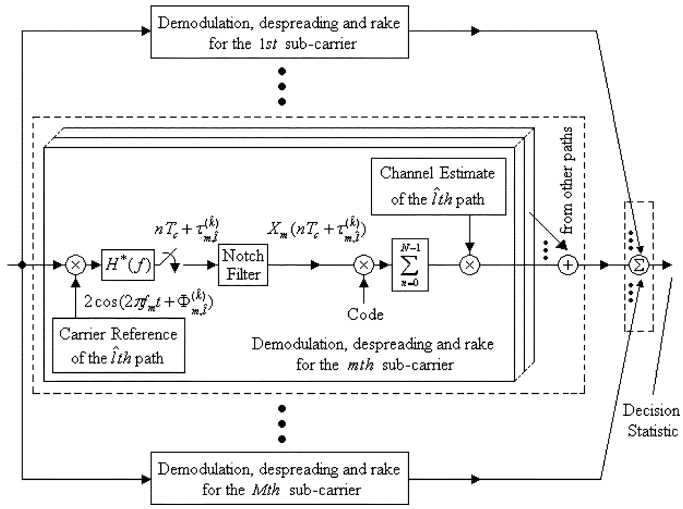

Fig. 6. Receiver for the kth user of the MC-CDMA UWB system.

a despreader. Similarly, the output of the despreader can be approximated as a Gaussian random variable with the SINR in the rth branch given by [14]

$$\gamma_{1,r}^{(m)} = \left\{ \frac{1}{2N^2} \left[\sum_{\substack{l=1 \\ l \neq r}}^{L_{\mathrm{MC}}} \Omega_{k,l} + (K-1) \right] \sum_{w_1=-W}^{W} \sum_{w_2=-W}^{W} \alpha_{w_1}^{(m)} \times \alpha_{w_2}^{(m)} \sum_{n=0}^{N-1} \sum_{\hat{n}=0}^{N-1} R(w_1 - \hat{n} + n, w_2 - \hat{n} + n) + \frac{M}{N\hat{p}(1+\vartheta)} \cdot \hat{\sigma}_J^2 \cdot \frac{J}{P} + M \left(\frac{E_b}{\eta_o} \right)^{-1} \sum_{w=-W}^{W} \left(\alpha_w^{(m)} \right)^2 \right\}^{-1} \tag{28}$$

and in the absence of NBI [14]

$$\gamma_{2,r}^{(m)} = \left\{ \frac{1}{2N^2} \left[\sum_{\substack{l=1 \\ l \neq r}}^{L_{\mathrm{MC}}} \Omega_{k,l} + (K-1) \right] \times \sum_{n=0}^{N-1} \sum_{\hat{n}=0}^{N-1} R(n - \hat{n}, n - \hat{n}) + M \left(\frac{E_b}{\eta_o} \right)^{-1} \right\}^{-1} \tag{29}$$

where N is the spreading factor of one subcarrier. $R(w_1 - \hat{n} + n, w_2 - \hat{n} + n)$ is defined as

$$R(n_1, n_2) = \int_0^1 x(\tau T_{\mathrm{ch}} - n_1 T_{\mathrm{ch}}) x(\tau T_{\mathrm{ch}} - n_2 T_{\mathrm{ch}}) d\tau \tag{30}$$

where $x(t)$ is the impulse response of a raised cosine filter and T_{ch} is the chip rate. In (28), $\hat{\sigma}_J^2$ is given by

$$\hat{\sigma}_J^2 = \int_{(1+\vartheta)(\hat{q}-\hat{p})/T_{\mathrm{ch}}}^{(1+\vartheta)(\hat{q}+\hat{p})/T_{\mathrm{ch}}} |H_w(f)|^2 |H(f)|^2 df. \tag{31}$$

$\hat{p}$ and $\hat{q}$ are defined, respectively, as a ratio of bandwidth of the narrowband interferer to the bandwidth of one subband, and a

ratio of the difference in center frequencies (between the narrowband interferer and the corrupted subband) to the bandwidth of one subband.

The despreader output is weighted by a channel estimate, and the weighted outputs from all branches are summed to form the final test statistics

$$\gamma = \sum_{m=1}^{M}\sum_{r=1}^{R}\beta_{m,r}^2\gamma_r^{(m)} = \gamma_1\beta_{M_1} + \gamma_2\beta_{M-M_1} \tag{32}$$

where M_1 is the number of subbands with NBI. In (32), γ_1 and γ_2 stand for the mean of the average SINR, excluding the attenuation factor, for all selected paths from all the subbands with and without NBI, respectively. They are numerically expressed as

$$\gamma_1 = \frac{1}{M_1 R}\sum_{m=1}^{M_1}\sum_{r=1}^{R}\gamma_{1,r}^{(m)} \tag{33}$$

$$\gamma_2 = \frac{1}{(M-M_1)R}\sum_{m=M_1+1}^{M}\sum_{r=1}^{R}\gamma_{2,r}^{(m)}. \tag{34}$$

$\zeta_{M_1} = \sum_{m=1}^{M_1}\sum_{r=1}^{R}\beta_{m,r}^2$ is defined as the sum of the square of the attenuation factors for the subcarriers with narrowband interferers, and $\zeta_{M-M_1} = \sum_{m=M_1+1}^{M}\sum_{r=1}^{R}\beta_{m,r}^2$ denotes the sum of the reminders. The BER for the MC-CDMA system thus can be expressed as

$$\begin{aligned} P_e &= \int_0^\infty Q(\sqrt{\gamma})p(\gamma)d\gamma \\ &= \int_0^\infty\int_0^\infty Q\left(\sqrt{\gamma_1\zeta_{M_1}+\gamma_2\zeta_{M-M_1}}\right) \\ &\qquad \times p\left(\zeta_{M_1}\right)p\left(\zeta_{M-M_1}\right)d\zeta_{M_1}d\zeta_{M-M_1} \end{aligned} \tag{35}$$

where $p(x)$ denotes log-normal pdf.

The TH-IR and MC-CDMA systems are compared under the conditions of same signal power, same data rate, and same bandwidth. The total bandwidth of the MC-CDMA UWB system is approximately

$$B_{\text{uwb}} \approx M\cdot(1+\vartheta)/T_{\text{ch}}. \tag{36}$$

Assuming that only one narrowband interferer is present, the parameters describing the NBI for the TH-IR UWB system and MC-CDMA system can be related as

$$\hat{p} = B_j/(B_{\text{uwb}}/M) \approx p\cdot M \tag{37}$$

$$\hat{q} = \frac{f_j - f_m}{(B_{\text{uwb}}/M)} \approx \frac{q}{|q|}\left[q\cdot M - \lfloor q\cdot M\rfloor - \frac{1}{2}\right]. \tag{38}$$

V. Numerical Results

Some representative numerical results of the TH-IR UWB in the presence of NBI are illustrated first in this section. The following system parameters are assumed unless explicitly specified: the pulse width T_p of the Gaussian monocycle; the modulation index ε; and the duration T_c of the time bin are 1.0, 0.2, and 2.0 ns, respectively [7]. The number N_s of pulses transmitted per symbol is five, the number N_h of time slots per frame is eight, and the number K of active users is eight. For the channel response, the number of multipaths L is 30, where the decay rate ν and the standard derivation σ are set at 0.15 and 0.5, respectively.

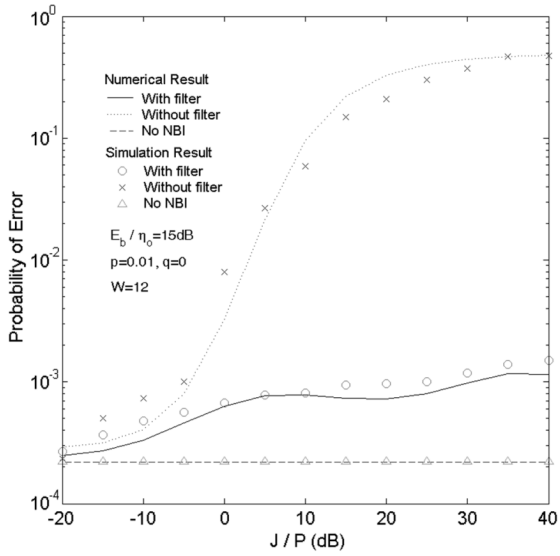

Fig. 7. Error probability as a function of interference power to signal power ratio.

Fig. 7 shows error probabilities for receiver with and without a notch filter as a function of J/P. For comparison, the case without NBI is also shown. Simulation and analytical results are presented under these conditions: $E_b/\eta_o = 15$ dB, $p = 0.01$, $q = 0$, $R = 10$, and $W = 12$. It can be seen from the figure that the performance without a notch filter degrades dramatically as J/P increases, especially when J/P is larger than 0 dB. When J/P is small (less than 0 dB), performances with and without notch filter are very close, so the notch filter is unnecessary. When J/P increases from 0 dB, the performance gap between filter and no-filter increases. When J/P is larger than 10 dB, by using the notch filter, two to three orders of magnitude of improvement are indicated. It can be observed that the analytic results and simulation results are close.

Fig. 8 investigates the system performance by exploring multipath diversity (Rake receiver) for different values of signal-to-noise ratio (SNR) ($E_b/\eta_o = 10$, 15, and 20 dB). Other parameters are $J/P = 30$ dB, $p = 0.01$, $q = 0$, and $W = 12$. It can be seen that for a given E_b/η_o, the error probability decreases sharply when the number of Rake fingers increases at the beginning ($R \leq 10$), then performance improvement becomes small when R approaches L. This indicates that reliable symbol decisions can be achieved by using a limited number of significant paths, rather than all paths.

The effect of the number of notch-filter taps on system performance is presented in Fig. 9 for $p = 0.01$, $E_b/\eta_o = 15$ dB, $J/P = 30$ dB, $q = 0$, and $R = 10$. It can be seen that the curves show a zig-zag shape in performance, rather than a smooth fall. This is because a further addition of taps, although providing better NBI suppression, introduces more pulse interference to the decision statistics, which is mainly due to the increase of

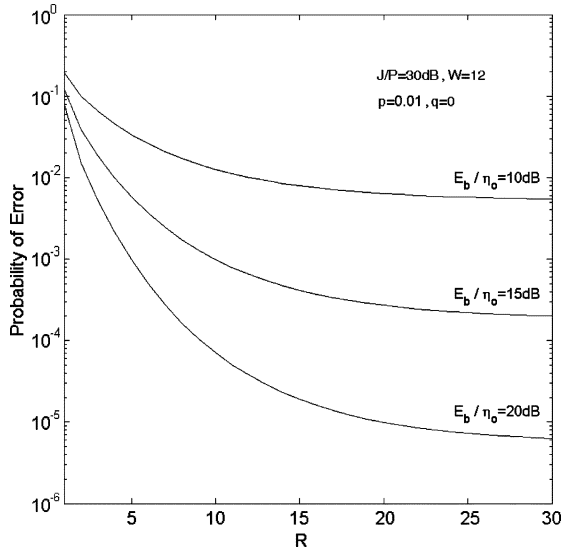

Fig. 8 BER for different Rake complexities.

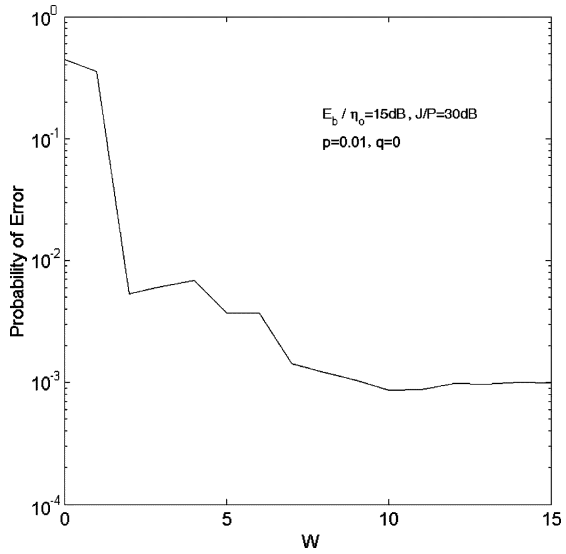

Fig. 9. System performance corresponding to different numbers of taps per side of the notch filter.

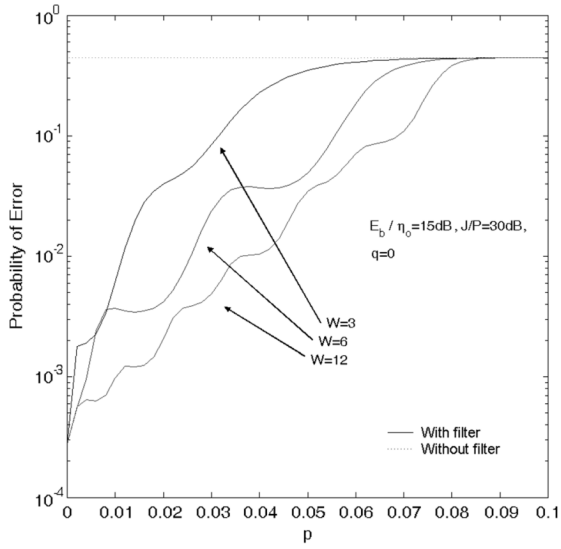

Fig. 10. Error probability versus the bandwidth ratio.

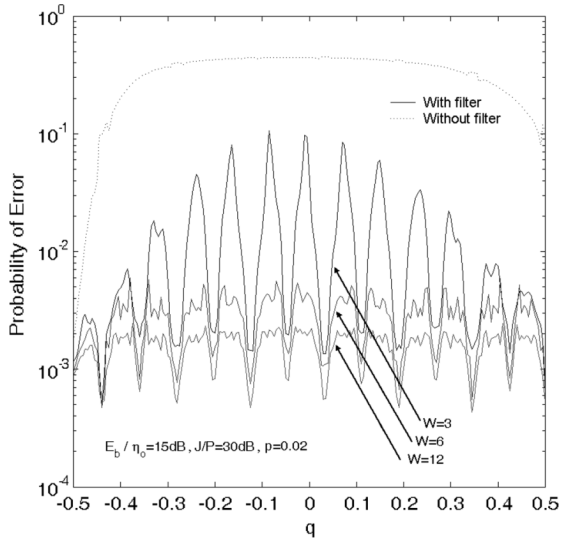

Fig. 11. System performance as the center frequency of the NBI varies.

probability of capturing pulses from multipath and multiple-access users. This phenomenon is serious when W is small, as the limited benefit of NBI reduction is counterbalanced or well exceeded by the worsening pulse interference. However, the overall trend of performance improvement continues as more taps are used. The curve levels off when $W > 8$, which indicates that the marginal improvement is limited. The error rates converge to different levels for different bandwidth ratios.

Figs. 10 and 11 are plotted against bandwidth ratio p (for $q = 0$) and the ratio q (for $p = 0.02$) of the offset of the center frequency of the narrowband interferer to the bandwidth, respectively. The remaining system parameters are set at $J/P =$ 30 dB with $E_b/\eta_o = 15$ dB. In accordance to the observation from Fig. 9, the notch filter with larger W offers greater resistance to the increase of the bandwidth ratio. From Fig. 11, it can be observed that the system performance varies for different normalized frequency offsets. The frequency response of the notch filter can be written as

$$H_W(f) = \sum_{w=-W}^{W} \alpha_w \exp(-j2\pi f w T_c). \tag{39}$$

Such variations can be accounted for by the periodicity and sinusoidal characteristics of the frequency response of the filter, as illustrated in Fig. 3. Better jamming rejection can be achieved when the center frequency of the narrowband system coincides with certain harmonics of $1/T_c$. The degree of accuracy of the estimating function depends on the number of taps per side of the notch filter. Notch filter with $W = 6$ offers better protection than that with $W = 3$, but the reliability of the decision statistic is unstable as q varies. However, when W is increased to 12, the sensitivity of the error rate subjected to the change of q is reduced significantly. The rate and fluctuation of the bit error can be reduced by using a filter of larger W.

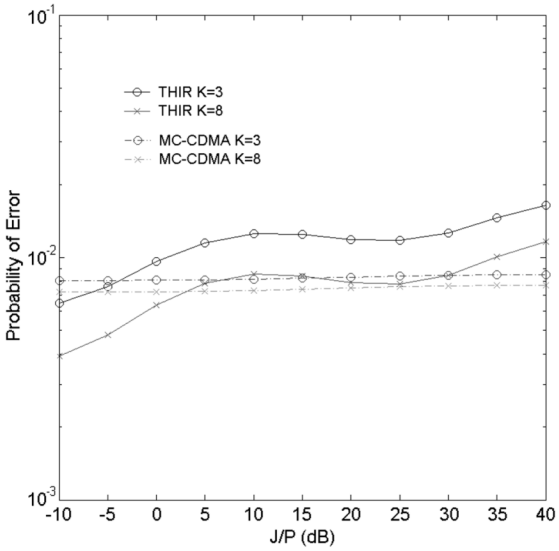

Fig. 12. Performance comparison between TH-IR and MC-CDMA UWB systems.

Fig. 12 compares the performances of TH-IR and MC-CDMA UWB systems subject to the change in J/P. The symbol time for the TH-IR and MC-CDMA systems, respectively, are given by $T_s = N_s N_h T_c$ and $T_s = NT_{\rm ch}$. It is assumed that the rolloff factor ϑ of the raised-cosine filter is 0.3, then the chip period $T_{\rm ch}$ is 10 ns, the spreading gain per subcarrier N is eight, and the number of subcarriers M is ten. For the channel response, the number of multipaths $L_{\rm MC}$ is three, where the decay rate $\nu_{\rm MC}$ and the standard derivation $\sigma_{\rm MC}$ have the values of 1.5 and 0.5, respectively. Only one narrowband signal is assumed within the spectrum of the system signal. When the corresponding ratios are $p = 0.01$ and $q = 0.05$, respectively, for the TH-IR system, for MC-CDMA system, the corresponding bandwidth ratio and normalized offset ratio are $\hat{p} = 0.1$ per (37) and $\hat{q} = 0$ per (38), respectively. In the absence of the near–far effect by assuming perfect power control for both systems, the SNR E_b/η_o is 10 dB, and the conditions for the number of active users K being three and eight are illustrated. For the TH-IR system, the parameters W and R are kept unchanged at 12 and 10, respectively. For the MC-CDMA system, the number of taps per side of the notch filter W is also 12. The number of correlators per subcarrier R is one, so as to maintain the same degree of diversity as the TH-IR system (10/30) in decision combining. Theoretically, the relative advantage of the MC-CDMA system over the TH-IR system is that the MC-CDMA system can enjoy frequency diversity of the branches unaffected by the narrowband system. For the MC-CDMA system, the impact of the jamming signal can be isolated within certain subbands. However, as observed, the use of a notch filter for TH-IR provides much performance improvement. Subjected to change in E_b/η_o, the performance difference between the TH-IR and MC-CDMA systems is limited.

VI. Conclusions

In this paper, performance expressions are derived for the TH-IR UWB communication system with transversal-type notch filtering at the receiver front-end. Results show that the use of a notch filter can provide significant improvement in system performance in various situations. Comparison between TH-IR and MC-CDMA UWB systems is also made. Under certain conditions, a relatively low-complexity TH-IR UWB system with notch filtering at the front end of the receiver is capable of achieving a similar BER to MC-CDMA.

Appendix A
Derivation of the Variances of MPI

Undesired pulses from multipath and multiple access can be collectively defined as interfering pulses to the reference path of the first user. The possibility for sampling of the interfering pulse is due to the combinational effect of random-coded time shifts, random propagation time delays, and the sampling time at the receiver. Considering the $\hat{n}$th sampling instant for the first user, the relative delay of the nth pulse from the lth path of the kth user with respect to the rth path of the first user can be expressed as

$$\begin{aligned}\tau_{k,l}^{(n)} &= \tau_{1,r} + \hat{n}T_c - nT_c - \tau_{k,l} \\ &= \lambda_{k,l}T_c + \Lambda_{k,l}^{(n)}T_c + \Delta_{k,l}^{(n)}T_f \end{aligned} \tag{A1}$$

where $\lambda_{k,l} \in [0,1)$, $\Lambda_{k,l}^{(n)} \in [0, N_h - 1]$, and $\Delta_{k,l}^{(n)} \in \{0,1,\ldots,\infty\}$. The template pulse for the rth correlator of the reference user and the interfering pulse from the lth path of the kth may overlap when $\Lambda_{k,l}^{(n)} = 0$ or when the pulses are within the same time bin. When $\Lambda_{k,l}^{(n)} \neq 0$, no overlapping exists.

The MPI $Z_{{\rm MPI}|r}$ takes the form

$$\begin{aligned} &Z_{{\rm MPI}|r} \\ &= \beta_{1,r}\psi_{1,r}\sum_{\substack{l=1\\ l\neq r}}^{L}\psi_{1,l}\beta_{1,l} \\ &\quad\times\sum_{n=0}^{N_s-1}\left\{\sum_{w=-W}^{W}\alpha_w\int_0^{T_c} s_1\big(t-\tau_{1,l}-wT_c+nT_f \right. \\ &\qquad\left. +c_1^{(n)}T_c+\tau_{1,r}\big)v(t)dt\right\} \\ &= \sqrt{E_1}\beta_{1,r}\psi_{1,r}\sum_{\substack{l=1\\ l\neq r}}^{L}\psi_{1,l}\beta_{1,l}\sum_{n=0}^{N_s-1}I_{{\rm MPI}|r}(l,n) \end{aligned} \tag{A2}$$

where $I_{{\rm MPI}|r}(l,n)$ can be written as

$$\begin{aligned} I_{{\rm MPI}|r}(l,n) = \sum_{w=-W}^{W}\alpha_w\int_0^{T_c}\Xi\Big(&t-\lambda_{1,l}T_c-\Lambda_{1,l}^{(n)}T_c \\ &-\Delta_{1,l}^{(n)}T_f-\varepsilon d_1^{\lfloor (n)/N_s\rfloor}\Big)\,v(t)dt \end{aligned} \tag{A3}$$

where $\lambda_{1,l}^{(n)}$, $\Lambda_{1,l}^{(n)}$, and $\Delta_{1,l}^{(n)}$ are given by

$$\begin{aligned} \lambda_{1,l} = \Big(&\tau_{1,l}-\tau_{1,r}+wT_c-nT_f-c_1^{(n)}T_c-\Delta_{1,l}^{(n)}T_f \\ &-\Lambda_{1,l}^{(n)}T_c\Big)/T_c \end{aligned} \tag{A4}$$

$$\begin{aligned} \Lambda_{1,l}^{(n)} = \Big\lfloor\Big(&\tau_{1,l}-\tau_{1,r}+wT_c-nT_f-c_1^{(n)}T_c \\ &-\Delta_{1,l}^{(n)}T_f\Big)/T_c\Big\rfloor \end{aligned} \tag{A5}$$

$$\Delta_{1,l}^{(n)} = \Big\lfloor\Big(\tau_{1,l}-\tau_{1,r}+wT_c-nT_f-c_1^{(n)}T_c\Big)/T_f\Big\rfloor. \tag{A6}$$

The integral in (A3) is non-zero only when the pulses are overlapped. Obviously, $\Lambda_{1,l}^{(n)}=0$ leads to $\lfloor(\tau_{1,l}-\tau_{1,r})/T_c\rfloor-c_1^{(n)}=-w$, where the sum on the left-hand side of the expression takes the same probability of $1/N_h$ for any possible value of arithmetic modulo N_h (i.e., $0,1,\ldots,N_h-1$). The probability of $\lfloor(\tau_{1,l}-\tau_{1,r})/T_c\rfloor-c_1^{(n)}=-w$ is given by

$$\text{Prob}\left(\lfloor(\tau_{1,l}-\tau_{1,r})/T_c\rfloor-c_1^{(n)}=-w\right)=\left(\frac{1}{N_h}\right)^2(N_h-|w|)\,. \tag{A7}$$

Thus the variance of the MPI term is

$$\begin{aligned}
&\text{Var}[Z_{\text{MPI}|r}]\\
&\quad=E\left[\left(\psi_{1,r}\beta_{1,r}\sum_{\substack{l=1\\l\neq r}}^{L}\psi_{1,l}\beta_{1,l}\sqrt{E_1}\sum_{n=0}^{N_s-1}I_{\text{MPI}|r}(l,n)\right)^2\right]\\
&\quad=E_1\beta_{1,r}^2\left(\sum_{\substack{l=1\\l\neq r}}^{L}\Omega_{1,l}\right)\\
&\qquad\times\left(\sum_{n_1=0}^{N_s-1}\sum_{n_2=0}^{N_s-1}E\left[I_{\text{MPI}|r}(n_1)I_{\text{MPI}|r}(n_2)\right]\right)
\end{aligned}\tag{A8}$$

where $E[I_{\text{MPI}|r}(n_1)I_{\text{MPI}|r}(n_2)]$ can be expressed as different forms corresponding to the values of n_1 and n_2. When $n_1=n_2$

$$\begin{aligned}
&E\left[I_{\text{MPI}|r}(n_1)I_{\text{MPI}|r}(n_2)\right]\\
&\quad=\left(\sum_{w=-W}^{W}\frac{N_h-|w|}{N_h^2}\alpha_w^2\right)\\
&\qquad\cdot\left\{\int_0^1\left[\frac{1}{2}\left(\int_0^{T_c}\Xi(t-\lambda T_c)v(t)dt\right)^2\right.\right.\\
&\qquad\left.\left.+\frac{1}{2}\left(\int_0^{T_c}\Xi(t-\lambda T_c-\varepsilon)v(t)dt\right)^2\right]d\lambda\right\}.
\end{aligned}\tag{A9}$$

When $n_1\neq n_2$

$$\begin{aligned}
&E\left[I_{\text{MPI}|r}(n_1)I_{\text{MPI}|r}(n_2)\right]\\
&\quad=\left(\sum_{w_1=-W}^{W}\sum_{w_2=-W}^{W}\left(\frac{N_h-|w_1|}{N_h^2}\right)\left(\frac{N_h-|w_2|}{N_h^2}\right)\alpha_{w_1}\alpha_{w_2}\right)\\
&\qquad\cdot\left\{\int_0^1\left[\frac{1}{2}\left(\int_0^{T_c}\Xi(t-\lambda T_c)v(t)dt\right)^2\right.\right.\\
&\qquad\left.\left.+\frac{1}{2}\left(\int_0^{T_c}\Xi(t-\lambda T_c-\varepsilon)v(t)dt\right)^2\right]d\lambda\right\}.
\end{aligned}\tag{A10}$$

Therefore, the variance of $Z_{\text{MPI}|r}$ can be written as

$$\text{Var}[Z_{\text{MPI}|r}]=\beta_{1,r}^2E_1\sigma_{\text{MPI}|r}^2 \tag{A11}$$

where

$$\begin{aligned}
\sigma_{\text{MPI}|r}^2&=\left(\sum_{\substack{l=1\\l\neq r}}^{L}\Omega_{1,l}\right)\\
&\quad\times\left\{\sum_{n_1=0}^{N_s-1}\sum_{n_2=0}^{N_s-1}E\left[I_{\text{MPI}|r}(n_1)I_{\text{MPI}|r}(n_2)\right]\right\}.
\end{aligned}\tag{A12}$$

Appendix B
Derivation of the Variances of MAI

The MAI $Z_{\text{MAI}|r}$ can be written as

$$\begin{aligned}
Z_{\text{MAI}|r}&=\beta_{1,r}\psi_{1,r}\sum_{k=2}^{K}\sum_{l=1}^{L}\psi_{k,l}\beta_{k,l}\\
&\quad\times\sum_{n=0}^{N_s-1}\left\{\sum_{w=-W}^{W}\alpha_w\int_0^{T_c}s_k\big(t-\tau_{k,l}-wT_c+nT_f\right.\\
&\qquad\left.+c_1^{(n)}T_c\big)v(t)dt\right\}\\
&=\beta_{1,r}\psi_{1,r}\sum_{k=2}^{K}\sqrt{E_k}\sum_{l=1}^{L}\psi_{k,l}\beta_{k,l}\\
&\quad\times\sum_{n=0}^{N_s-1}I_{\text{MAI}|r}(k,l,n)
\end{aligned}\tag{B1}$$

where $I_{\text{MAI}|r}(k,l,n)$ is given by

$$\begin{aligned}
I_{\text{MAI}|r}(k,l,n)&=\sum_{w=-W}^{W}\alpha_w\int_0^{T_c}\Xi\Big(t-\lambda_{k,l}T_c-\Lambda_{k,l}^{(n)}T_c\\
&\qquad-\Delta_{k,l}^{(n)}T_f-\varepsilon d_k^{\lfloor n/N_s\rfloor}\Big)v(t)dt
\end{aligned}\tag{B2}$$

where $\lambda_{k,l}^{(n)}$, $\Lambda_{k,l}^{(n)}$, and $\Delta_{k,l}^{(n)}$ are given by

$$\begin{aligned}
\Delta_{k,l}^{(n)}&=\Big\lfloor\big(\tau_{k,l}-\tau_{1,r}+wT_c-nT_f\\
&\qquad+c_k^{(n)}T_c-c_1^{(n)}T_c\big)\Big/T_f\Big\rfloor
\end{aligned}\tag{B3}$$

$$\begin{aligned}
\Lambda_{k,l}^{(n)}&=\Big\lfloor\Big(\tau_{k,l}-\tau_{1,r}+wT_c-nT_f+c_k^{(n)}T_c\\
&\qquad-c_1^{(n)}T_c-\Delta_{k,l}^{(n)}T_f\Big)\Big/T_c\Big\rfloor
\end{aligned}\tag{B4}$$

$$\begin{aligned}
\lambda_{k,l}&=\Big(\tau_{k,l}-\tau_{1,r}+wT_c-nT_f+c_k^{(n)}T_c\\
&\qquad-c_1^{(n)}T-\Delta_{k,l}^{(n)}T_f-\Lambda_{k,l}^{(n)}T_c\Big)\Big/T_c.
\end{aligned}\tag{B5}$$

Similarly, the integral in (B2) has a nonzero value only when $\Lambda_{k,l}^{(n)}=0$, or alternatively, $\lfloor(\tau_{k,l}-\tau_{1,r})/T_c\rfloor+c_k^{(n)}-c_1^{(n)}=-w$. Again, the sum takes the same probability of $1/N_h$ for any value in the set $[0,1,\ldots,N_h-1]$. The probability of pulse overlapping is given by

$$\begin{aligned}
&\text{Prob}\left(\lfloor(\tau_{k,l}-\tau_{1,r})/T_c\rfloor+c_k^{(n)}-c_1^{(n)}=-w\right)\\
&\qquad=\left(\frac{1}{N_h}\right)^2(N_h-|w|)\,.
\end{aligned}\tag{B6}$$

$$
\begin{aligned}
&\mathrm{Var}(Z_{\mathrm{NBI}|r}) \\
&= \beta_{1,r}^2 \sum_{n_1=0}^{N_s-1}\sum_{n_2=0}^{N_s-1}\Bigg\{ \sum_{w_1=-W}^{W}\sum_{w_2=-W}^{W}\alpha_{w_1}\alpha_{w_2}\int_0^{T_c}\int_0^{T_c} E\Big[j\left(t_1+\tau_{1,r}+n_1T_f+c_1^{(n_1)}T_c-w_1T_c\right) \\
&\qquad\qquad \cdot j\left(t_2+\tau_{1,r}+n_2T_f+c_1^{(n_2)}T_c-w_2T_c\right)\Big]v(t_1)v(t_2)dt_1dt_2\Bigg\} \\
&= J\cdot\beta_{1,r}^2 \sum_{n_1=0}^{N_s-1}\sum_{n_2=0}^{N_s-1}\Bigg\{ \sum_{w_1=-W}^{W}\sum_{w_2=-W}^{W}\alpha_{w_1}\alpha_{w_2} \\
&\qquad\qquad \cdot\left[\int_0^{T_c}\int_0^{T_c} E\left\{\overline{R}_j\left[t_1-t_2+(n_1-n_2)T_f+\left(c_1^{(n_1)}-c_1^{(n_2)}\right)T_c-(w_1-w_2)T_c\right]\right\}\cdot v(t_1)v(t_2)dt_1dt_2\right]\Bigg\} \\
&= J\cdot\beta_{1,r}^2 \sum_{n_1=0}^{N_s-1}\sum_{n_2=0}^{N_s-1} I_{\mathrm{NBI}|r}(n_1,n_2)
\end{aligned}
\tag{C2}
$$

Thus, the variance of the MAI term is

$$
\begin{aligned}
&\mathrm{Var}[Z_{\mathrm{MAI}|r}] \\
&= E\left[\left(\beta_{1,r}\psi_{1,r}\sum_{k=2}^{K}\sum_{l=1}^{L}\psi_{k,l}\beta_{k,l}\sqrt{E_k}\right.\right. \\
&\qquad \left.\left.\times\sum_{n=0}^{N_s-1} I_{\mathrm{MAI}|r}(k,l,n)\right)^2\right] \\
&= \beta_{1,r}^2\sum_{k=2}^{K}E_k\left(\sum_{l=1}^{L}\Omega_{k,l}\right) \\
&\quad\times\left(\sum_{n_1=0}^{N_s-1}\sum_{n_2=0}^{N_s-1}E\left[I_{\mathrm{MAI}|r}(n_1)I_{\mathrm{MAI}|r}(n_2)\right]\right)
\end{aligned}
\tag{B7}
$$

where $E[I_{\mathrm{MAI}|r}(n_1)I_{\mathrm{MAI}|r}(n_2)]$, has a different form for different n_1 and n_2. For $n_1 = n_2$

$$
\begin{aligned}
&E\left[I_{\mathrm{MAI}|r}(n_1)I_{\mathrm{MAI}|r}(n_2)\right] \\
&= \left(\sum_{w=-W}^{W}\frac{N_h-|w|}{N_h^2}\alpha_w^2\right) \\
&\quad\times\left\{\int_0^1\left[\frac{1}{2}\left(\int_0^{T_c}\Xi(t-\lambda T_c)v(t)dt\right)^2\right.\right. \\
&\qquad\left.\left.+\frac{1}{2}\left(\int_0^{T_c}\Xi(t-\lambda T_c-\varepsilon)v(t)dt\right)^2\right]d\lambda\right\}.
\end{aligned}
\tag{B8}
$$

For $n_1 \neq n_2$

$$
\begin{aligned}
&E\left[I_{\mathrm{MAI}|r}(n_1)I_{\mathrm{MAI}|r}(n_2)\right] \\
&= \left(\sum_{w_1=-W}^{W}\sum_{w_2=-W}^{W}\left(\frac{N_h-|w_1|}{N_h^2}\right)\left(\frac{N_h-|w_2|}{N_h^2}\right)\alpha_{w_1}\alpha_{w_2}\right) \\
&\quad\cdot\left\{\int_0^1\left[\frac{1}{2}\left(\int_0^{T_c}\Xi(t-\lambda T_c)v(t)dt\right)^2\right.\right. \\
&\qquad\left.\left.+\frac{1}{2}\left(\int_0^{T_c}\Xi(t-\lambda T_c-\varepsilon)v(t)dt\right)^2\right]d\lambda\right\}.
\end{aligned}
\tag{B9}
$$

Therefore, the variance of $Z_{\mathrm{MAI}|r}$ is

$$
\mathrm{Var}(Z_{\mathrm{MAI}|r}) = \beta_{1,r}^2\left(\sum_{k=2}^{K}E_k\right)\sigma_{\mathrm{MAI}|r}^2 \tag{B10}
$$

where

$$
\sigma_{\mathrm{MAI}|r}^2 = \left\{\sum_{n_1=0}^{N_s-1}\sum_{n_2=0}^{N_s-1}E\left[I_{\mathrm{MAI}|r}(n_1)I_{\mathrm{MAI}|r}(n_2)\right]\right\}. \tag{B11}
$$

Appendix C
Derivation of the Variance of NBI

The NBI $Z_{\mathrm{NBI}|r}$ is given by

$$
\begin{aligned}
Z_{\mathrm{NBI}|r} = \beta_{1,r}\psi_{1,r}\sum_{n=0}^{N_s-1}\Bigg\{\sum_{w=-W}^{W}\alpha_w\int_0^{T_c} j\big(t+\tau_{1,r}-wT_c \\
+nT_f+c_1^{(n)}T_c\big)v(t)dt\Bigg\}
\end{aligned}
\tag{C1}
$$

with variance as shown in (C2) at the top of the page. Since $\{c_1^{(n)}\}$ is a random sequence and each element takes the same probability of $1/N_h$ for any value of $0, 1, \ldots, N_h-1$, the probability of $c_1^{(n_1)} - c_1^{(n_2)} = m, m \in [-(N_h-1), N_h-1]$, is given by

$$
P\left(c_1^{(n_1)}-c_1^{(n_2)}=m\right) = \left(\frac{1}{N_h}\right)^2(N_h-|m|). \tag{C3}
$$

$I_{\mathrm{NBI}|r}(n_1,n_2)$ can be expressed as different forms based on the values of n_1 and n_2.

For $n_1 = n_2$

$$I_{\mathrm{NBI}|r}(n_1,n_2) = \sum_{w_1=-W}^{W}\sum_{w_2=-W}^{W}\alpha_{w_1}\alpha_{w_2} \times \int_0^{T_c}\int_0^{T_c}\overline{R}_j\left[t_1 - t_2 - (w_1-w_2)T_c\right]v(t_1)v(t_2)dt_1dt_2. \quad \text{(C4)}$$

For $n_1 \neq n_2$

$$I_{\mathrm{NBI}|r}(n_1,n_2) = \sum_{w_1=-W}^{W}\sum_{w_2=-W}^{W}\alpha_{w_1}\alpha_{w_2} \times \sum_{m=-(N_h-1)}^{N_h-1}\left\{\left(N_h - |m|/N_h^2\right)\int_0^{T_c}\int_0^{T_c}\overline{R}_j\left[t_1 - t_2 + (n_1-n_2)T_f + mT_c - (w_1-w_2)T_c\right]v(t_1)v(t_2)dt_1dt_2\right\}. \quad \text{(C5)}$$

Thus, $\mathrm{Var}(Z_{\mathrm{NBI}|r})$ is given by

$$\mathrm{Var}(Z_{\mathrm{NBI}|r}) = J\beta_{1,r}^2\sigma_{\mathrm{NBI}|r}^2 \quad \text{(C6)}$$

where

$$\sigma_{\mathrm{NBI}|r}^2 = \sum_{n_1=0}^{N_s-1}\sum_{n_2=0}^{N_s-1} I_{\mathrm{NBI}|r}(n_1,n_2). \quad \text{(C7)}$$

ACKNOWLEDGMENT

The authors would like to thank Professor L. B. Milstein at the University of California, San Diego, for his pointing out the topic at the early stage of this research.

REFERENCES

[1] R. A. Scholtz, "Multiple access with time-hopping impulse modulation," in *Proc. IEEE Milcom*, 1993, pp. 447–450.
[2] M. Win and R. A. Scholtz, "Ultra-wide bandwidth time-hopping spread spectrum impulse radio for wireless multiple access communications," *IEEE Trans. Commun.*, vol. 48, no. 4, pp. 679–691, Apr. 2000.
[3] M. Win and R. A. Scholtz, "Impulse radio: How it works," *IEEE Commun. Lett.*, vol. 2, no. 1, pp. 10–12, Jan. 1998.
[4] L. Zhao and A. Haimovich, "Performance of ultra-wideband communications in presence of interference," *IEEE J. Sel. Areas Commun.*, vol. 20, no. 12, pp. 1684–1691, Dec. 2002.
[5] M. Hamalainen, V. Hovinen, R. Tesi, J. Iinatti, and M. Latva-aho, "On the UWB system coexistence with GSM900, UMTS/WCDMA and GPS," *IEEE J. Sel. Areas Commun.*, vol. 20, no. 12, pp. 1712–1721, Dec. 2002.
[6] D. Laney, G. M. Maggio, F. Lehmann, and L. Larson, "Multiple access for UWB impulse radio with pseudochaotic time hopping," *IEEE J. Sel. Areas Commun.*, vol. 20, no. 12, pp. 1692–1700, Dec. 2002.
[7] F. Ramirez-Mireles, "Signal design for ultra-wideband communications in dense multipath," *IEEE Trans. Veh. Technol.*, vol. 51, no. 6, pp. 1517–1521, Nov. 2002.
[8] J. T. Conroy, J. L. LoCicero, and D. R. Ucci, "Communication techniques using monopulse waveforms," in *Proc. IEEE Milcom*, 1999, pp. 1181–1185.
[9] "FCC first report and order regarding ultra-wideband transmission systems," Order (FCC 02-48), Apr. 22, 2002.
[10] I. Bergel, E. Fishler, and H. Messer, "Narrowband interference suppression in time-hopping impulse-radio systems," in *Proc. IEEE Conf. Ultra Wideband Syst. Technol.*, May 2002, pp. 303–307.
[11] T. T. Wong and J. Wang, "MMSE receiver for multicarrier CDMA overlay in ultra-wideband communications," *IEEE Trans. Veh. Technol.*, vol. 54, no. 2, pp. 603–614, Mar. 2005.
[12] L. B. Milstein *et al.*, "On the feasibility of a CDMA overlay for personal communications networks," *IEEE J. Sel. Areas Commun.*, vol. 10, no. 5, pp. 655–668, May 1992.
[13] H. V. Poor, "Active interference suppression in CDMA overlay systems," *IEEE J. Sel. Areas Commun.*, vol. 19, no. 1, pp. 4–20, Jan. 2001.
[14] J. Wang and L. B. Milstein, "Multicarrier CDMA overlay for ultra-wideband communications," *IEEE Trans. Commun.*, vol. 52, no. 10, pp. 1664–1669, Oct. 2004.
[15] ——, "CDMA overlay situations for microcellular mobile communications," *IEEE Trans. Commun.*, vol. 43, no. 2–4, pp. 603–614, Feb.–Apr. 1995.
[16] J. Foerster, "Channel modeling sub-committee report (final)," IEEE P802.15 Working Group for Wireless Personal Area Networks, IEEE P802.15, Dec. 2002.
[17] L. B. Milstein, "Interference rejection techniques in spread spectrum communications," *Proc. IEEE*, vol. 76, no. 6, pp. 657–671, Jun. 1988.
[18] S. C. Schwartz and Y. S. Yeh, "On the distribution and moments of power sums with log-normal components," *Bell Syst. Tech. J.*, vol. 61, no. 7, pp. 1441–1462, Sep. 1982.

Jiangzhou Wang (M'91–SM'94) received the B.S. and M.S. degrees from Xidian University, Xian, China, in 1983 and 1985, respectively, and the Ph.D. degree (with Greatest Distinction) from the University of Ghent, Ghent, Belgium, in 1990, all in electrical engineering.

Dr. Wang is currently a Professor and Chair in the Department of Electronics, University of Kent, Kent, U.K. From 1995 to 2005, he was with the University of Hong Kong, where he is still serving as an Honorary Professor. From 1992 to 1995, he was a Senior System Engineer with Rockwell International Corporation (now Conexant), Newport Beach, CA. From 1990 to 1992, he was a Postdoctoral Fellow with the University of California at San Diego, CA. He held a Visiting Professor position with NTT DoCoMo, Japan. He has published over 140 papers, including more than 40 IEEE TRANSACTIONS/JOURNAL papers in the areas of wireless mobile and spread spectrum communications. He has written/edited two books, *Broadband Wireless Communications* (Boston, MA: Kluwer, 2001) and *Advances in 3G Enhanced Technologies for Wireless Communications* (Norwood, MA: Artech House, 2002). The latter book has been translated into Chinese. He holds one U.S. patent in the GSM system.

Dr. Wang is an Editor for IEEE TRANSACTIONS ON COMMUNICATIONS and a Guest Editor for IEEE JOURNAL ON SELECTED AREAS IN COMMUNICATIONS (Wideband CDMA, 2000 and 2001, and Advances in Multicarrier CDMA, 2006). He is listed in *Who's Who in the World* (New Providence, NJ: Marquis). He was a Technical Chairman of the IEEE Workshop in 3G Mobile Communications in 2000. He has been a Technical Committee Member and Session Chair for a number of international conferences.

Wong Tat Tung received the B. Eng. and M. Phil. degrees from the University of Hong Kong, Hong Kong, in 2001 and 2003, respectively.

From 2003 to 2004, he was a Research Assistant with the University of Hong Kong. He is now working for the Hong Kong Government. His research interests are in theory and techniques for wireless spread-spectrum communications.